Journal of Biomedical Optics 9(1), 139–148 (January/February 2004)

Macular pigment Raman detector for clinical applications

Igor Ermakov
Maia Ermakova
Werner Gellermann
University of Utah
Department of Physics and Dixon Laser Institute
Salt Lake City, UT 84112
E-mail: werner@physics.utah.edu

Paul S. Bernstein
Moran Eye Center
Department of Ophthalmology and Visual Sciences
Salt Lake City, UT 84132

Abstract. Clinical studies of carotenoid macular pigments (MP) have been limited by the lack of noninvasive, objective instruments. We introduce a novel noninvasive optical instrument, an MP Raman detector, for assessment of the carotenoid status of the human retina *in vivo*. The instrument uses resonant excitation of carotenoid molecules in the visible wavelength range, and quantitatively measures the highly specific Raman signals that originate from the single- and double-bond stretch vibrations of the π-conjugated carotenoid molecule's carbon backbone. The instrument is a robust, compact device and suitable for routine measurements of MP concentrations in a clinical setting. We characterized and tested the instrument in clinical studies of human subjects to validate its function and to begin to establish its role as a possible screening test for macular pathologies. We also show that the MP Raman spectroscopy technology has potential as a novel, highly specific method for rapid screening of carotenoid antioxidant levels in large populations at risk for vision loss from age-related macular degeneration, the leading cause of blindness of the elderly in the developed world. [DOI: 10.1117/1.1627776]

Keywords: age-related macular degeneration; macular pigments; lutein; zeaxanthin; Raman spectroscopy; noninvasive detector.

Paper 103008 received Mar. 19, 2003; revised manuscript received Jun. 26, 2003; accepted for publication Jul. 1, 2003.

1 Introduction

Age-related macular degeneration (AMD) is the leading cause of blindness in the developed world[1] and there is no effective treatment for the majority of patients with this disease. According to recent studies, the macular carotenoid pigments (MP) lutein and zeaxanthin might play a role in the treatment and prevention of AMD.[2] These pigments are concentrated in the macula lutea, a 5-mm diameter region of the retina that is essential for highest visual acuity and color vision. The mechanisms by which these two macular pigments, derived exclusively from dietary sources such as green leafy vegetables and orange-yellow fruits and vegetables, might protect against AMD are still unclear. These pigments are known to be excellent free-radical scavenging antioxidants in a tissue at high risk of oxidative damage owing to high levels of light exposure and to abundant highly unsaturated lipids.[1,3] In addition, since these molecules absorb in the blue-green spectral range, they act as filters that may attenuate photochemical damage caused by short-wavelength visible light reaching the retina.[4]

There is considerable interest in the noninvasive measurement of macular carotenoid levels in the elderly population to determine whether low levels of macular pigment are associated with increased risk of AMD.[5] Currently the most commonly used noninvasive method for measuring human macular pigment levels is a subjective psychophysical heterochromatic flicker photometry test involving color intensity matching of flickering blue and green light aimed at the fovea with the same light aimed at the perifoveal area.[6] This method is time intensive and requires an alert, cooperative subject with good visual acuity, and there may be high intrasubject variability when macular pigment densities are low or if significant macular pathology is present.[7] Thus the usefulness of this method for assessing macular pigment levels in the elderly population most at risk for AMD is severely limited. Nevertheless, researchers have used flicker photometry to investigate important questions such as variation of macular pigment density with age and diet. In a recent flicker photometry study, for example, the pigment density was found to increase slightly with age,[8] but another study found the opposite trend.[5] Several objective techniques for the measurement of macular pigment in the human retina have been explored recently as alternatives to the subjective psychophysical tests. The underlying optics principles of these techniques are based on either fundus-reflection[9,10] or fundus-fluorescence (autofluorescence) spectroscopy;[11] however, all of them suffer from numerous assumptions and limitations.[12]

Recently we demonstrated a novel optical approach to *in vivo* detection of MP[13,14] based on resonance Raman scattering. The technique is objective as well as noninvasive and appears to be fast and quantitative; its exquisite specificity means that it could be used for patients with a variety of ocular pathologies. In this paper we describe the underlying principles of the MP Raman technology and the instrument used for clinical MP measurements. We characterize the instrument, discuss the physical meanings of the data obtained, and discuss various potentially confounding measurement conditions. We show that the Raman technique holds promise

1083-3668/2004/$15.00 © 2004 SPIE

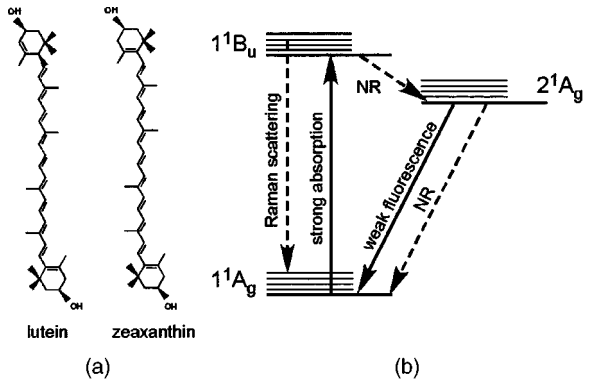

Fig. 1 (a) Chemical structure of lutein and zeaxanthin molecules. They differ in the location of the additional C=C bond in one ionone ring. (b) Energy-level diagram of long-chain carotenoid molecules with optical and nonradiative transitions.

for a major advance in the study and possibly the early diagnosis of macular degenerative diseases. Besides the retina, the technology can also be used as a potential early diagnostic test of disorders in human skin and the oral cavity.[15,16]

2 Optical Properties of Carotenoids

Lutein and zeaxanthin carotenoid molecules [Fig. 1(a)] are similar to polyenes in their structure and optical properties. Their carbon backbones contain nine alternating conjugated carbon double C=C and single C—C, bonds. The carbon backbone is terminated at each end by an ionone ring to which a hydroxyl group is attached. Four methyl groups are attached to the backbone as side groups. Zeaxanthin differs from lutein only in the location of one of the double bonds and in the stereochemistry of the 3′ carbon site.

An energy-level diagram of the carotenoid molecule is shown in Fig. 1(b). We use labels associated with the irreducible representations belonging to the C_{2h} point group to describe the symmetries of the electronic states of carotenoids. Human retinal tissue contains high concentrations of lutein and zeaxanthin. The absorption of these molecules and the monotonically decreasing scattering background account for the complete absorption behavior of the macula, as seen in Fig. 2. The strong electronic absorption occurs in a broad band (about an 80-nm width) centered at about 450-nm, and shows a clearly resolved vibronic substructure with a spacing of 1400 cm^{-1}. The absorption is caused by electric dipole-allowed vibronic transitions of the molecule's conjugated π-electron from the 1^1A_g singlet ground state to the 1^1B_u singlet excited state [see Fig. 1(b)]. Optical excitation within the absorption band leads to weak luminescence (not shown, peak at 530-nm, width 50-nm) with a small Stokes shift, which again shows vibronic substructure.

By analogy with that of the well-studied β-carotene molecule, the extremely low quantum efficiency of the lutein-zeaxanthin luminescence is caused by the existence of a second excited singlet state, a 2^1A_g state, which lies below the 1^1B_u state. Following optical excitation of the 1^1B_u state, the energy relaxes rapidly (within approximately 200–250 fs in β-carotene[17]) by nonradiative transitions to the lower 2^1A_g state, from which electronic emission to the ground state is

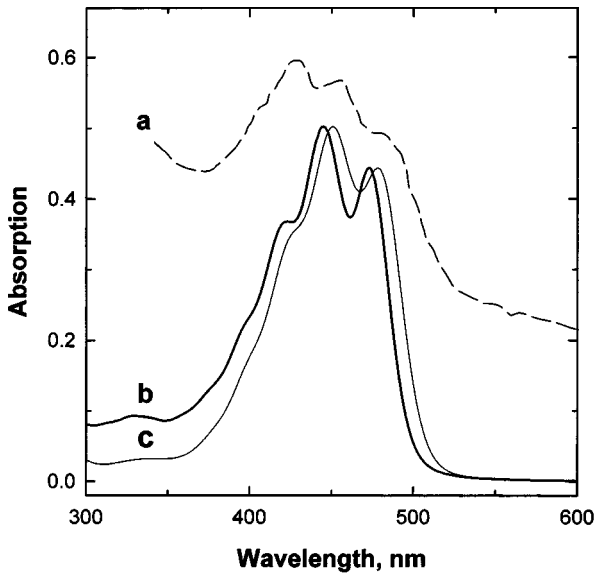

Fig. 2 Absorption spectra of excised, flat-mounted human retina (curve a), lutein (curve b), and zeaxanthin (curve c) dissolved in methanol. Note the remarkable similarity of the retinal tissue absorption to the absorption of carotenoid solutions.

symmetry forbidden. The extremely low luminescence $1^1B_u \rightarrow 1^1A_g$ and the absence of $2^1A_g \rightarrow 1^1A_g$ fluorescence of lutein-zeaxanthin allow us to measure the resonant Raman scattering response of the molecules without potentially interfering intrinsic fluorescence signals.

The Raman spectrum of carotenoid molecules, shown in Fig. 3, is characterized by two prominent Stokes lines at 1159 and 1524 cm^{-1}, originating, respectively, from the C—C single-bond and the C=C double-bond stretch vibrations of the conjugated backbone. A weaker peak at 1008 cm^{-1} is attributed to the rocking motion of the molecule's methyl side groups.[18] As is evident from Fig. 3, both lutein and zeaxanthin have very similar resonance Raman spectra in terms of Raman shifts and peak widths at room temperature. The Raman signals are superimposed on a weak fluorescence background originating from intrinsic $1^1B_u \rightarrow 1^1A_g$ carotenoid fluores-

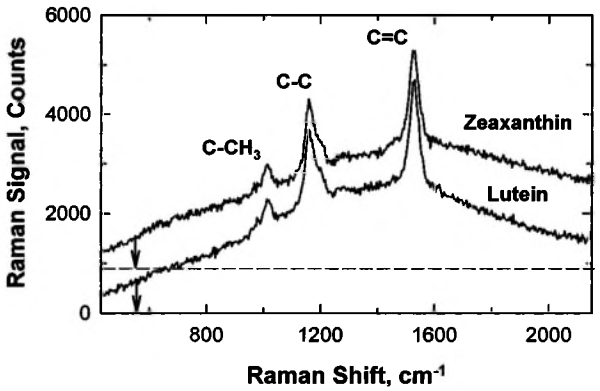

Fig. 3 Resonant Raman spectrum of methanol solution of zeaxanthin and lutein measured under excitation with a 488-nm argon laser line. The horizontal dashed line indicates zero for the Raman spectrum of zeaxanthin, which was shifted by 900 counts for the sake of clarity.

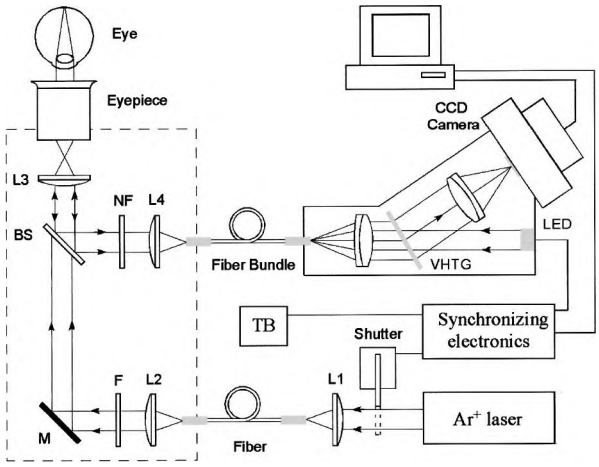

Fig. 4 The setup of the fiber-based MP Raman detector, an instrument for quantitative measurements of macular carotenoid pigment content in clinical settings.

cence that varies slightly in spectral shape and strength, depending on the type of carotenoid molecule. In all cases the intensity ratio between Raman signal and background fluorescence is about 0.8:1 at the spectral position of the C=C Raman peak. We also found that Raman signal intensity is proportional to the concentration of the molecules in optically thin solvents, as is expected for a linear spectroscopic technique like Raman spectroscopy. Therefore the Raman peak height can be used as a measure of the carotenoid content of optically thin samples.

3 Raman Detector and Computer Interface

Initially we used Raman spectroscopy to measure flat-mounted human retinas and excised eye cups.[19] For the measurement of living human eyes, the ocular light exposure during a measurement must be limited to prevent both photochemically and thermally induced retinal injury, as specified by the safety regulations of the American National Standards Institute. Furthermore, for an instrument to be useful in a clinical setting, it needs to be highly specific, sensitive, and robust. To meet all these requirements, we developed a compact, portable, fiber-based, and computer-interfaced Raman instrument. The layout of this MP Raman detector is shown schematically in Fig. 4. The instrument sacrifices unneeded spectral resolution for the benefit of increased light throughput. Also, it can be interfaced to a fundus camera to help monitor the delivery of the excitation laser beam to the foveal area of the retina in living eyes. The instrument consists of a beam delivery and collection optics module mounted on a kinematic positioning system, a small argon laser, a Raman spectrograph coupled with a thermoelectric cooled CCD camera, controlling electronics, and a computer interface.

The beam delivery and collection optics module is shown in the lower left part of Fig. 4. The excitation laser beam originates from a small air-cooled argon laser operating on the 488-nm line. It is routed via an optical fiber into the module, collimated by lens L2, transmitted through filter F, and reflected by mirror M; it then passes through a dichroic beamsplitter BS, and is finally imaged onto the macula by a combination of an auxiliary lens L3, and an eyepiece. The laser-excitation fiber is a multimode fiber with a core diameter of 550 μm and a numerical aperture NA=0.22. The dielectric bandpass filter F, which is placed in the excitation path, blocks any spectral components outside a narrow 3-nm bandwidth centered around the 488-nm excitation wavelength. This blocking effectively suppresses fiber fluorescence and laser plasma lines in the Raman-scattering spectral range of interest. The Raman-scattered, wavelength-shifted light is collected in 180-deg backscattering geometry with the same eyepiece-lens combination used to deliver the excitation beam and is reflected by the dichroic beamsplitter into a separate light collection path. A holographic rejection notch filter NF, which effectively blocks the Rayleigh light components of the scattered light occurring at the excitation wavelength, is placed in this path prior to coupling the Raman-scattered light with a collection fiber using lens L4. The holographic rejection notch filter NF suppresses the excitation light by six orders of magnitude while transmitting the Raman-shifted light components with 80% efficiency. The light collection fiber is a fiber bundle consisting of 96 individual multimode fibers, each with a 70-μm core diameter, and higher than 55% overall transmission owing to a high fiber filling factor. The input cross-section of the fiber bundle is circular (1-mm diameter) and the output cross-section is rectangular (70 μm×8.6 mm) to match the rectangular input slit geometry of a homemade spectrograph designed for high light throughput.

The spectrograph employs two achromatic lenses for light collimation and a volume holographic transmission grating (VHTG). The line density of the VHTG is 1200 mm^{-1}, and the diffraction efficiency is higher than 80% for nonpolarized light. The *f*-number of the spectrograph is 2 and thus is ideally matched to the *f*-number of the individual multimode fibers comprising the fiber bundle.

The dispersed spectrum is imaged onto the 8.63×6.53-mm silicon chip (Texas Instruments, model TC-241) of a CCD camera (Santa Barbara, Inc., model ST6v). The CCD chip consists of an array of 750×121 pixels, each having an area 11.5×27 μm. It has a relatively low detector noise, with a combined dark and readout noise smaller than about 8 counts. The quantum efficiency of this chip in the blue-green spectral range of interest is about 55%. We chose to vertically bin pixels oriented perpendicular to the dispersion plane of the spectrograph into "super pixels" and thus achieved simultaneously a low readout noise (24 counts per super pixel) and a high readout speed (0.5 s per spectrum). The resolution limit of our Raman spectrograph is about 20 cm^{-1}.

The MP Raman detector has several provisions to aid in the optical alignment of the instrument for the human eye. An optical shutter is designed so that even in the closed state a very small portion of the blue argon laser light used for Raman excitation is transmitted. A subject looking into the instrument thus sees a blue spot originating from the end face of the excitation light delivery fiber. Using a proper choice of focal lengths for lenses L2, L3, and the eyepiece, we realized a 1:2 magnification, effectively imaging the excitation fiber end face into a 1-mm diameter spot on the retina. Furthermore, using a low-power light-emitting diode (LED), we generated an additional red polka-dot pattern, originating from the facets of the light collection fiber bundle as an alignment aid for the subject. With the focal length of lens L4 chosen to be twice that of lens L2, the 1-mm circular face of the red

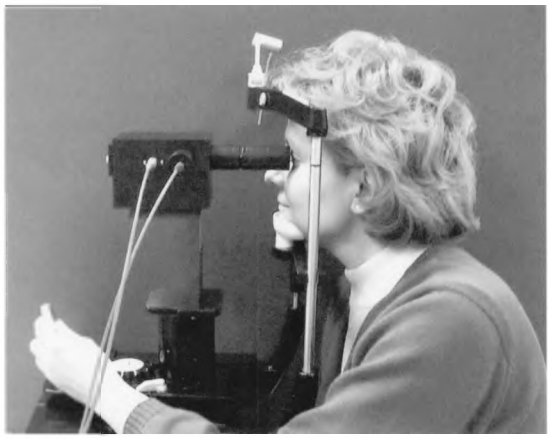

Fig. 5 Measuring MP level. The subject looks into the instrument and adjusts the optical alignment while resting the forehead against the device.

illuminated fiber bundle is imaged at the patient's retina as a 1-mm spot and thus has a slightly smaller diameter than the blue illuminated retinal excitation spot.

The use of the MP Raman detector is illustrated in Fig. 5. Prior to a measurement, the subject overlaps the blue disk and the red polka-dot pattern, as shown in Fig. 6, to ensure proper alignment of his or her eye with respect to the instrument. This alignment is achieved by suitable positioning of the head. The subject can wear his or her usual glasses or contact lenses if needed (see later discussion regarding their influence on the Raman response). After the subject has signaled alignment, the instrument operator pushes a trigger button. The synchronized electronics momentarily turns off the red LED aiming beam to avoid exposure of the CCD detector, opens the shutter to allow laser light to project onto the retina, and triggers the data acquisition system. After a preset measurement time of 0.25 s, the instrument closes the laser shutter, digitizes the backscattered light, downloads the data into computer memory, and initiates software processing for spectral display.

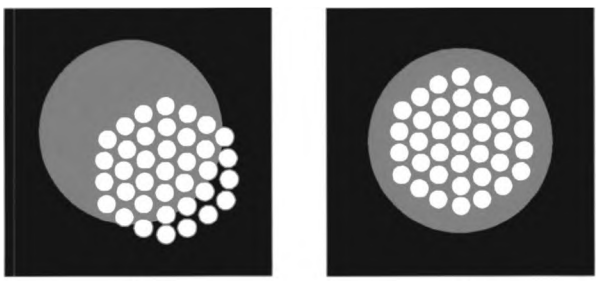

Fig. 6 Procedure for alignment of the Raman instrument with the optical axis of the subject's eye. The subject sees two colored light patterns when looking into the instrument: a weak blue circular disk from the argon laser fiber (shown in gray) and a weak red polka-dot pattern originating from an LED-illuminated light-collection fiber bundle. Alignment is achieved when the subject moves his or her head so that both patterns overlap. (a) Misaligned; (b) aligned.

The instrument is interfaced to a small personal computer with home-developed Windows-based software for data acquisition and processing. All post-exposure processing takes only 0.25 s, and thus the instrument provides an almost instantaneous display of the final Raman spectrum and other operating parameters on the computer monitor after each measurement. Using the Windows-based computer interface, the software facilitates a number of other functions. It permits the operator to properly initiate the hardware, and it establishes all necessary communication between the computer and the CCD camera. It automatically measures the dark spectrum and subtracts it whenever a "light" measurement is made; processes the spectra; saves the data as text ASCII files; and finally prompts the operator to properly shut down the instrument.

4 Safety Considerations

To comply with ANSI safety regulations, the ocular exposure levels used in our Raman instrument have to stay below certain specified threshold levels. According to the latest issue, ANSI Z136.1-2000,[20] ocular exposure levels have to be limited to protect the eye from both photochemically and thermally induced retinal injury under measurement conditions (visible light near 0.5 μm, immobilized eyes, exposure time of 0.25 s). The photochemical limit for retinal injury (Sec. 8.3.1 of the ANSI guidelines) is listed as 2.7 C_B J/cm^2, where C_B is a wavelength correction factor, and results in 15.5 J/cm^2 with $C_B=5.75$ for 488-nm. The thermal limit for retinal injury (Sec. 8.3.2), valid for an exposure time of $0.07<t<0.7$ s, has to be calculated from the laser spot present at the cornea and is listed as $1.8(\alpha/1.5)t^{0.75}$ mJ/cm^2. Here α is the angle of the laser source at the location of the viewer, measured in milliradians. Using $t=0.07$ s and $\alpha=58.8\times10^{-3}$ rad, we obtain an energy density of 9.6 mJ/cm^2 at the cornea for the thermal exposure limit of the retina.

In a typical single-exposure measurement with our instrument (0.25-s ocular exposure with 1 mW light at 488-nm), a total laser energy of 0.25 mJ is projected onto an 8-mm-diameter spot at the cornea and a 1-mm-diameter spot on the retina. This corresponds to a retinal exposure level of 32 mJ/cm^2, which is 480 times lower than the 15.5 J/cm^2 photochemical limit. For the ocular exposure used, we calculate a level of 0.5 mJ/cm^2 considering that the light energy of 0.25 mJ is distributed over a spot with an 8-mm diameter at the cornea; therefore this exposure level is 19 times lower than the thermal limit of 9.6 mJ/cm^2 for retinal injury.

5 Raman Measurements

The appearance of the computer monitor after a typical measurement is shown in Fig. 7. On the left side of the screen a safety and dosimetry control table is displayed. This table shows the exposure dose as a function of the excitation laser power and exposure time chosen, and the area of the excitation spot on the retina. It also contains the ratio of the light dose with respect to the maximum permissible exposure dose. As can be seen from the table, under typical experimental conditions (exposure time 0.25 s, laser power 1 mW, spot size 1 mm), a safety factor of 19 is obtained.

The central part of the screen shows the measured Raman spectrum superimposed on a spectrally broad background

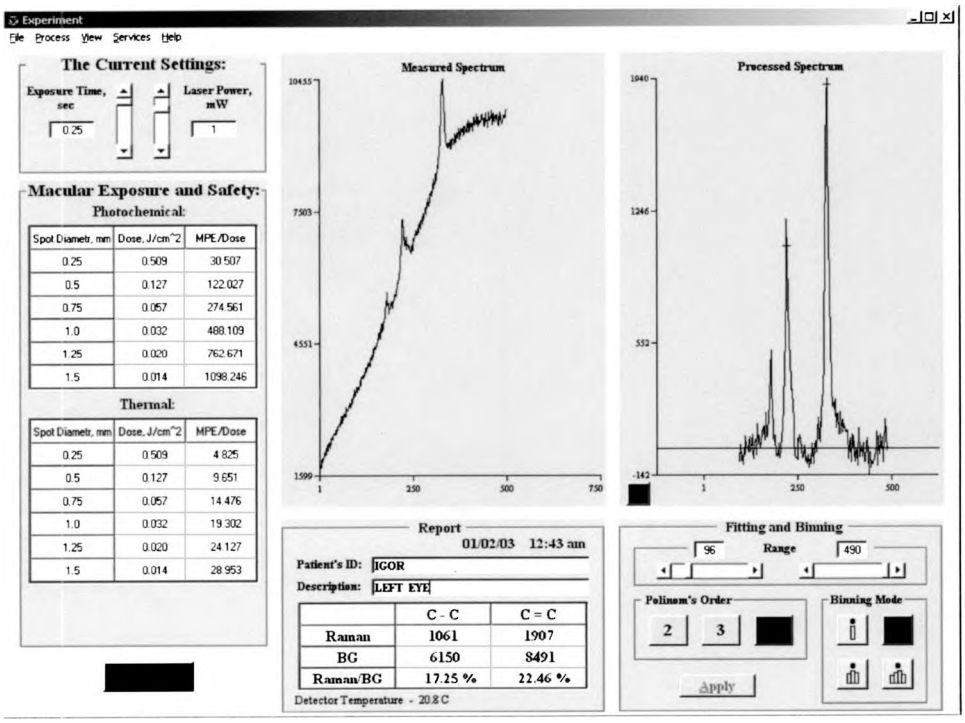

Fig. 7 Display of a typical Raman measurement of human MP on the computer monitor. See text for details.

spectrum caused by fluorescence of the retina. This spectrum is a difference spectrum resulting from the subtraction of a dark spectrum (recorded before a measurement) from the measured spectrum. The observer may view this spectrum to obtain general spectral information, i.e., the shape and height of the combined fluorescence-Raman spectra.

The right part of the screen displays the measured carotenoid Raman spectrum after subtraction of the overlapping fluorescence background, which is accomplished by polynomial fitting of the background spectrum and subsequent subtraction from the spectrum displayed in the central window. To derive the shape of the background, we use all data points in the selected wavelength range except those in the vicinity of the Raman peaks. All these data points are curve fitted to a user-selected polynomial of up to the fourth order, and the computed polynomial curve is subtracted from the original spectrum. This results in a curve containing spectral information exclusively from the Raman response of the macular carotenoids. We found that the shapes of the lutein and zeaxanthin spectra were not distinguishable from the shape of human MP Raman spectra.

To obtain an accurate reading of the Raman peak heights, we eliminated the influence of potentially overlapping noise spikes in the spectrum by fitting the measured Raman line shapes with Lorentzians in a single-parameter fit, where we used the known wavelength positions and (instrumentation-broadened) spectral widths of the Raman peaks of interest. The calculated values for the intensities of the C—C single-bond and C═C double-bond peaks, along with the values for the fluorescence intensity under those peaks, and the ratios of the Raman intensities to the background, are tabulated in a report window (see the lower middle part of Fig. 7). The final peak height of the C═C double bond signal at 1524 cm^{-1} is chosen as a measure of carotenoid concentration. To aid in clinical studies, this window allows one to enter the subject's personal data; it contains a dated time stamp and it saves this information along with the spectra.

If needed, it is possible to improve the quality of the spectrum, i.e., the signal-to-noise ratio, by summing over up to four neighboring pixels in a binning-mode option (lower right part of Fig. 7). Furthermore, markers indicating the signal strength for Raman peaks and the baseline can be used to evaluate the quality of the data processing.

The spectral details of an MP measurement obtained with the instrument are summarized in Fig. 8 and Table 1. Spectrum a in Fig. 8 was obtained from a human macula and spectrum c is the amplitude-adjusted spectrum from zeaxanthin dissolved in ethanol. Spectrum b in Fig. 8 represents the difference between macular and authentic zeaxanthin spectra and therefore has to be assigned to the fluorescence spectrum of an "unpigmented" retina. According to the literature,[21] this fluorescence is most likely due to lipofuscin, a major retinal fluorophore located in the retinal pigmented epithelium (RPE) cells, whose function in the eye has not as yet been defined. According to the retinal spectrum decomposition, only 21% of the signal intensity is contributed by the MP Raman signal; the remaining fractions, 27 and 52%, originate from carotenoid and lipofuscin fluorescence, respectively. Obviously, the ratio of the carotenoid Raman signal to carotenoid fluorescence under a fixed-excitation wavelength will remain the same in any macula. However, the fraction of lipofuscin fluorescence in the macular spectrum might vary from person to person, depending on several factors, such as MP content and age. The age factor is essential since the human retina supposedly accumulates lipofuscin with increasing age.[21]

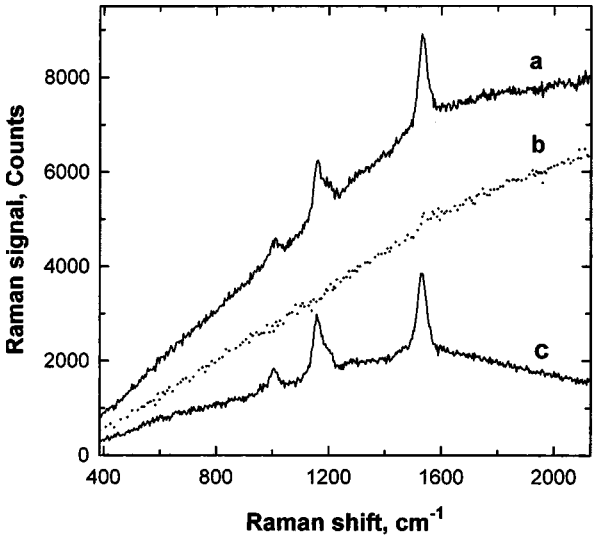

Fig. 8 Spectral decomposition of a typical macular spectrum, (curve a) indicating the contributions of retinal autofluorescence (curve b) and a carotenoid Raman spectrum (curve c).

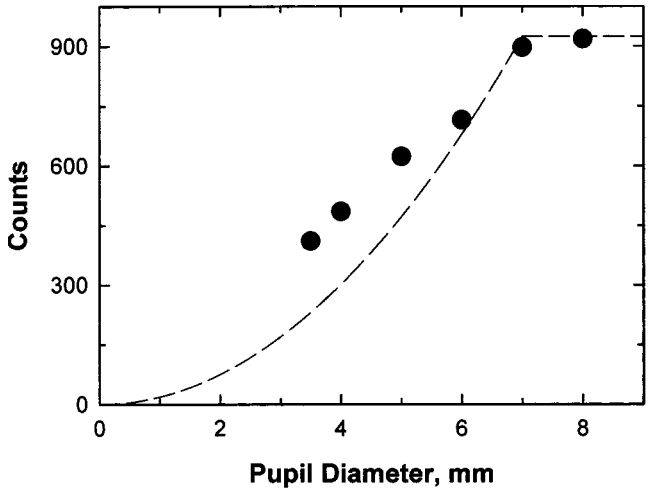

Fig. 9 Measured variation in the Raman signal with pupil diameter for a human subject (circles). The dashed curve is the theoretically expected change in the signal with pupil diameter. Above a 7-mm pupil diameter, the signal stays constant (see text).

6 Pupil Diameter and Raman Intensity

It is useful to show how the pupil diameter would affect the Raman signals measured with the instrument. The dependence of the Raman response on pupil diameter d can be understood by considering the geometric light throughput of the instrument, F_{inst}, which is designed with an effective aperture of 7 mm (defined by the magnified aperture of the light-collection fiber bundle), and the light throughput of the eye, F_{eye}, which scales quadratically with pupil diameter. Both result in the overall throughput of the system (eye plus MP detector): $F_{\text{syst}}=\min\{F_{\text{inst}},F_{\text{eye}}\}$, which is indicated in Fig. 9. The instrument aperture limits the overall light throughput to $F_{\text{syst}}=F_{\text{inst}}$ for $d\geqslant 7$ mm. The light throughput of the eye is given by $F_{\text{eye}}=kd^2$, where k is a constant accounting for the transmission properties of the average human eye. The total light throughput of the system is thus controlled by the pupil diameter for the case $d<7$ mm, and it is limited by F_{instr} when d exceeds a 7-mm diameter.

In one set of measurements, the subject was measured repeatedly while his pupil was dilated pharmacologically. Between measurements the pupil's diameter was measured in ambient light. As shown in Fig. 9, the carotenoid Raman C=C peak intensity (circles) gradually increases as the pupil slowly dilates to its maximum diameter, leveling off at about 7 mm. In the fully dilated state, for some individuals the signals can be twice as large as in the undilated state.

The data in Fig. 9 reveal that measured signal levels are noticeably higher than the levels for pupil diameters below 6 mm. This effect appears because the incompletely dilated pupil is still changing its diameter while it is being measured. When initially exposed to the bright excitation beam, the eye reflex contracts the pupil from a dark-adapted large diameter to a smaller diameter determined by the counteracting effects of light intensity and progressing pharmacological immobilization. Since light exposure and pupil reaction time are comparable (~0.25 s), the effective pupil diameter is higher than the diameter measured under ambient light conditions (which is shown as the abscissa in Fig. 9). As a consequence of these pupil diameter effects, for clinical instrumentation trials we chose to measure only fully dilated (pupil diameter 7 to 8 mm), immobilized eyes of subjects, thus ensuring maximized light throughput as well as consistent measuring conditions under bright-light exposure.

Table 1 Signal components of a typical MP Raman measurement.

Signal	Intensity	Percentage
Retina fluorescence (lipofuscin)	4604	52%
Carotenoid fluorescence	2361	27%
Carotenoid Raman signal	1889	21%
Overall signal	8854	100%

7 Instrument Calibration

To find a correlation between the Raman readings and the actual carotenoid content of the living macula, we conducted calibration experiments using thin, 1-mm path length quartz cuvettes filled with carotenoid solutions and placed them in a focal plane of a positive lens with a focal length of 22 mm. Such a lens is known to approximate the refractive properties of a human eye. The effective excitation volume then is a cylinder with a length of 1.0 mm and a base diameter of 1.1 mm (the diameter of a laser beam), resulting in a sampling volume of about 1 μl. As calibration materials we initially chose freshly prepared ethanol solutions of zeaxanthin and lutein with varying but known carotenoid content in the 1-μl sampling volume and corresponding to the average carotenoid concentrations typically found in excised human macular samples (as measured by high pressure liquid chromatography). Also, we measured the absorption of these samples with a precison UV/visible spectrometer.

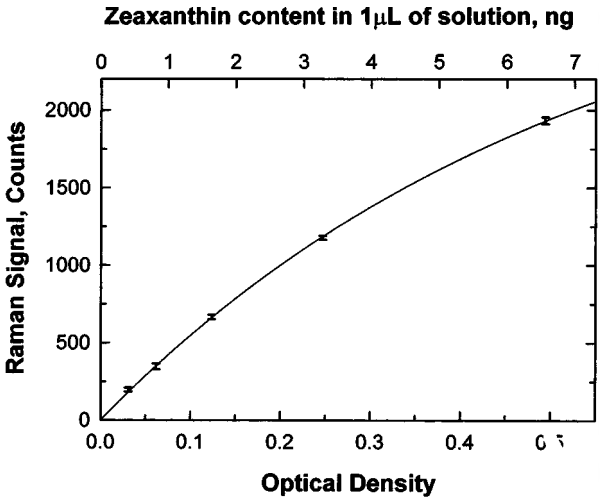

Fig. 10 Calibration curve of the MP Raman detector linking the instrument reading with the carotenoid content in a human macula. The curve was obtained using a model eye discussed in the text containing zeaxanthin dissolved in methanol. The sampling volume, 1 μl, corresponds to a 1-mm-diameter spot at a macula and contains carotenoid typical for a human macula.

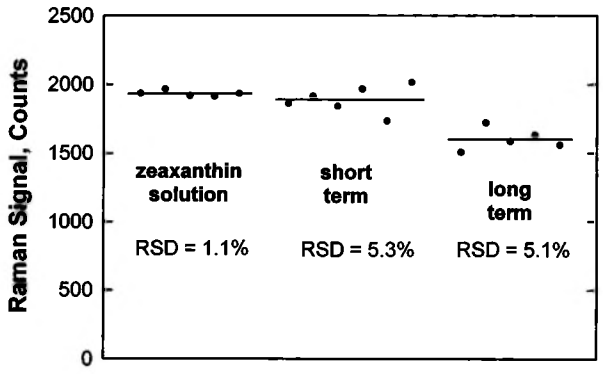

Fig. 11 Repeatability of Raman measurements. The left part represents data for zeaxanthin solution in a model eye. The central and right data represent the short-term and long-term repeatability of macular pigment measurements for two different subjects. The Raman intensities for the long-term dataset were measured over a 2-week period in five sessions.

Using the MP Raman detector described, the model eye, and the solutions, we obtained the calibration results shown in Fig. 10 for zeaxanthin (which is the predominant carotenoid in the central part of the human fovea). The concentration axis shown at the top of Fig. 10 indicates the carotenoid concentration calculated for the sampling volume using the published extinction coefficient for zeaxanthin.[22] The calibration curve for lutein (not shown) essentially coincides with that for zeaxanthin since both the Raman excitation efficiency and the extinction coefficient are virtually equal for both carotenoids. The calibration response directly correlates the Raman response (i.e., the C=C peak height) with the concentration of carotenoids and also shows that linear tracking of carotenoid concentrations is possible for low and moderate concentrations, as is the case for the living human macula.

A deviation from the linear response occurs, however, as expected, at higher MP densities, i.e., at MP densities in excess of an optical density >0.25 (measured at 450 nm) where self-absorption of the Raman-shifted light occurs. The measured calibration curve is not only useful for correcting MP Raman signals at higher concentrations, but also serves as a direct correlation between the Raman signal and average MP carotenoid content measured in nanograms per milliliter or correlated with the optical absorption coefficient and optical density.

It is important to note that MP optical density values for Raman spectroscopy and heterochromatic flicker photometry are not readily comparable. This is because the Raman method measures the carotenoid content averaged over the entire region illuminated by the 1-mm spot, whereas psychophysics measures the optical density only at the edge of the illumination spot.[6] Recent studies comparing the two techniques in the same subjects do confirm a significant correlation between them, however.

The calibration curve does not usually change during the lifetime of a particular Raman instrument and hence the data correction can be integrated into the instrumentation software. In particular, this means that the theoretically expected shape of the calibration curve

$$S(D) \approx A \times (1 - e^{-kD})$$

will remain the same for any given MP detector using a wavelength of 488-nm for the MP Raman signal excitation, but the amplitude of the curve, A, must be found for each instrument by performing the calibration procedure described earlier in order to ensure a cross-calibration between individual instruments.

8 Sources of Noise and Errors in MP Measurements

For daily sensitivity calibration purposes, instead of the degradable liquid carotenoid solutions, we developed a chemically and photostable solid-state alternative that is Raman active in the same spectral region as the carotenoid C—C and C=C stretch vibrations. This material is a thin slab of polished diamond, combined with a positive lens ($f = 22$ mm), and housed in a small, 30×35-mm cylinder attachable to the front end of the Raman instrument. The Raman intensity of the diamond material has the same order of magnitude as an average Raman signal from the human retina and its short-term (day-to-day) and long-term (month-to-month) stability was tested to be tighter than 1%. We obtained comparable accuracies also for zeaxanthin and lutein solutions in the model eye; i.e., relative standard deviations (RSDs) for five measurements were as low as 1.1% (see Fig. 11).

Regarding the noise and error analysis of the instrument, we list in Table 1 and Table 2 the Raman signal strengths obtained from the macula of a young human subject, along with the noise levels of the signals. Also, we list in Table 2 the expected noise components associated with photon and detector noise. The data allow one to conclude that the measurements are "photon limited" since the photon noise, N_{ph}, exceeds the detector noise, N_D. Thus the main source of noise is the quantum mechanically limited photon noise or shot noise, which is unavoidable and is a part of a measurement. The signal contributions, listed in Table 1, indicate that the

Table 2 Sources of noise in the MP Raman detector.

Parameters			Value
CCD quantum efficiency		η	0.54
CCD analog to digital conversion gain,	e^-/count	g	3.35
Measured signal intensity,	count	$\eta \times I/g$	8854
Predicted photon noise,	count	$N_{ph}=\frac{1}{g}\sqrt{\eta \times I}$	51
Measured detector noise,	count	N_D	33
Predicted overall noise,	count	$\sqrt{N_D^2+\eta \times I/g^2}$	61
Measured overall noise,	count	N_Σ	65
Signal-to-noise ratio for C=C peak,		$\frac{\eta(I-I_{BG})}{gN_\Sigma}$	1889/65=29
Main source of noise			Photon noise

intensity of the useful carotenoid Raman signals is only 21% of the overall intensity of the measured spectrum. Therefore the main contribution to the photon noise comes from the fluorescence excited along with the carotenoid Raman signal. In spite of this disadvantage, the signal-to-noise ratio for the Raman response in a typical single experiment is very high (about 10 to 20), and can exceed a factor of 30 for subjects with high MP content.

To evaluate short-term repeatability in human MP measurements, we measured the MP in the same pupil-dilated eye six times with 3 to 4-min intervals between measurements. These time intervals ensured that afterimages from the laser exposure had faded. The results are shown in Fig. 11. The relative standard deviation was 5.3% for this dataset and thus about five times higher than the RSD for the ideal carotenoid sample (1.1%). Next, we repeated the MP measurements in five consecutive sessions for another subject over a 2-week period using pupil dilation for each set of measurements. In this case, the standard deviation was 5.1%. These results clearly demonstrate the high accuracy of the Raman instrument and prove that the RSDs in humans are always higher than the RSDs of carotenoid samples. This increased RSD effect obviously is due to the human factor, i.e., the measurement conditions deviate from the perfect optical alignment conditions. Each measurement of a human subject is affected by eye alignment errors, and the average value of these errors varies from person to person involved in the study, depending on factors such as visual acuity, fixation ability, and alignment experience. We observed a wide range of alignment errors, varying from 3 to 15%. Interfacing the Raman detector with a standard fundus camera could significantly reduce the alignment error since it would allow the operator to monitor the alignment quality so that measurements are initiates only when the eye is properly aligned. Another, practically quite useful alternative, is to accept datasets obtained from an individual MP measurement session only if the RSD stays within a reasonably low range.

9 Influence of Contact Lenses and Eyeglasses

Since a significant number of subjects might use correcting eyeglasses during measurements, we analyzed whether this would influence the MP results. We considered two major effects associated with thin lenses having no intrinsic absorption in the visible spectral range. One deals with Fresnel losses at the refracting surfaces. The reflected light from a single surface for normal incidence is given by[23]:

$$R=\left(\frac{n-1}{n+1}\right)^2,$$

where n is the refractive index of the lens. For uncoated lenses, the single-pass losses, $[R+R(1-R)]\approx 2R$, will be as high as 8% for CR 39 plastics ($n=1.498$), and 9.6 to 10.7% for the most commonly used high-index lenses (with refractive indices of 1.56 and 1.60). As a consequence, the Raman excitation will be reduced by 8 to 11% Fresnel losses, and the overall MP Raman response by about 16 to 22%. This situation is the worst-case scenario for uncoated eyeglasses. Currently, the eyeglass industry offers a wide variety of corrective eye wear, including lenses with antireflection (AR) coatings, scratch-resistant coatings, and photochromic lenses whose transmission varies with light intensity. This needs to be taken into account since the losses of AR-coated lenses could be as low as a few percent and could be neglected in most cases, while photochromic eyeglasses could attenuate the Raman signals by an order of magnitude. Unlike eyeglasses, contact lenses normally do not introduce any sizable effect because of the almost perfect index matching at the cornea–lens interface and owing to the comparable losses existing at the cornea–air and contact lens–air interfaces.

A second major influence on the Raman readings is caused by the fact that correction lenses change the size of the retinal images relative to the image size of the normal eye (magnification for positive power lenses and image reduction for

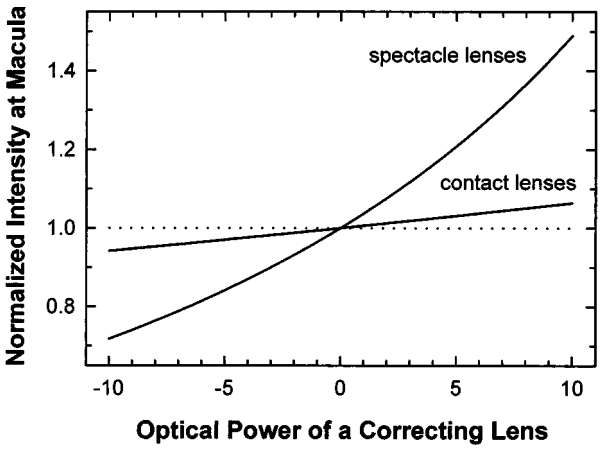

Fig. 12 Relative variation in the laser light intensity at the retina with the optical power of correcting spectacles or contact lenses. These curves should be used on a regular basis for adequate correction of MP Raman data when the subject has used his or her lenses during MP measurements.

negative power lenses). The magnitude of this effect depends on the respective lens power and its vertex distance h_e, specified as the distance from the correction lens to the eye's entrance pupil (and not to the cornea). Assuming that the lens is typically placed 15-mm in front of the cornea and that the entrance pupil's location is 3.05-mm inside the eye,[24] the value of the vertex distance will amount to $h_e = 15 + 3.05 = 18.05$ mm. Contact lenses can be treated in a similar manner, with a resulting vertex distance of about 3.05 mm ($h_e \approx 0 + 3.05 = 3.05$ mm). This nonvanishing vertex distance means that even contact lenses have a magnification effect, although it is much smaller than a corresponding eyeglass lens.

Using a ray-tracing program, we calculated the correction factors to be used for MP data obtained from subjects wearing myopic or hyperopic correction lenses. For myopic correction there is a reduction in image size, and for hyperopic correction there is an increase in image size compared with the normal eye. The measured Raman signal scales with the second power of the diameter of the retinal excitation spot since the Raman intensity is a linear function of power density. The resulting plot for the correction factor as a function of a correction lens power is shown in Fig. 12.

In Table 3, we summarize all the influences of optical correction devices discussed here that a subject might wear during MP measurements. In order to make the necessary corrections to the measured Raman data, the instrument operator simply looks up the type and characteristics of the correction optics and determines the product of correction factors using Fig. 12. It is clear from Table 3 that contact lenses are preferred over eyeglasses and that the instrument operator should encourage subjects to use contact lenses whenever possible. Indeed, as seen from Fig. 12, for moderate optical power of contact lenses (diopter ranging from −8 to +8) the correction factor for the Raman signal is less than several percent.

Table 3 Effects of optical correction on Raman signal.

	Correction Type	
Effects	Spectacle Lens	Contact Lens
Intrinsic losses	No	No
Fresnel losses	Up to 22% reduction in Raman signal	No
Magnification	Significant increase or reduction in Raman signal	Virtually small effect

10 First Clinical Results and Conclusion

The experiments described here, along with the recent validation trials we performed in our laboratories,[14,25] demonstrate that the MP Raman instrument is suitable for clinical environments. The test is easily performed by human subjects, even in the presence of significant macular pathologies. Measurement repeatability is high as long as the subjects have central fixation with a visual acuity of 20/80 or better. The test is rapid (0.25 s), and light exposure levels for the macula are well within established laser safety standards. Excitation light intensities are sufficiently high, however, to generate afterimages. This necessitates about a 2-min wait between exposures.

First clinical studies[25] carried out at the University of Utah's Moran Eye Center revealed that carotenoid Raman signal intensities declined with age in normal eyes. This decline is too strong to be entirely explainable as a decrease in ocular transmission with age.[12] A corroborating observation is the fact that younger subjects of similar ages (and comparable lens opacities) had drastically varying MP levels. These findings increase the potential usefulness of the MP Raman detection technology in screening young subjects for their levels of future AMD risk. Our studies also showed that average levels of lutein and zeaxanthin were 32% lower in AMD eyes compared with normal elderly control eyes as long as the subjects were not consuming high-dose lutein supplements. Patients who had begun to consume supplements containing high doses of lutein ($\geq$4 mg/day) regularly after their initial diagnosis of AMD had average MP levels that were in the normal range and that were significantly higher than in AMD patients not consuming these supplements.[25]

These findings are consistent with the hypothesis that low levels of MP in the human macula may represent a pathogenic risk factor for the development of AMD. Resonance Raman measurement of macular carotenoid pigments could play an important role in facilitating large-scale prospective clinical studies of lutein and zeaxanthin protection against AMD, and this technology may someday prove useful in the early detection of individuals at risk for visual loss from AMD.

In conclusion, we find that resonance Raman spectroscopy is a highly promising technology for the clinical measurement of macular carotenoid levels in living human subjects. It is noninvasive, precise, sensitive, specific, rapid, reproducible, and objective. Currently, the technology has been transferred to several independent research groups starting their own clinical trials. Clinical studies involving larger subject bases are under way, and it is hoped that they will help clarify the roles of lutein and zeaxanthin in the prevention and treatment of AMD.

Acknowledgments

This research was supported by funds from Spectrotek, L.C., the National Eye Institute (grants R29-EY11600, STTR 1 R41 EY12324-01, and STTR 2 R42 EY12324-02), and Research to Prevent Blindness, Inc.

References

1. W. Schalch, P. Dayhaw-Barker, and F. M. Barker, "The carotenoids of the human retina," in *Nutritional and Environmental Influences on the Eye*, A. Taylor, Ed., pp. 215–250, CRC Press, Boca Raton, FL (1999).
2. G. J. Handelman, D. M. Snodderly, A. J. Adler, M. D. Russett, and E. A. Dratz, "Measurement of carotenoids in human and monkey retinas," *Methods Enzymol.* **213**, 220–230 (1992).
3. S. Beatty, H.-H. Koh, D. Henson, and M. Boulton, "The role of oxidative stress in the pathogenesis of age-related macular degeneration," *Surv. Ophthalmol.* **45**, 115–134 (2000).
4. V. M. Reading and R. A. Weale, "Macular pigment and chromatic aberration," *J. Am. Optom. Assoc.* **64**, 231–234 (1974).
5. S. Beatty, I. J. Murray, D. B. Henson, D. Carden, H.-H. Koh, and M. E. Boulton, "Macular pigment and risk for age-related macular degeneration in subjects from a northern European population," *Invest. Ophthalmol. Visual Sci.* **42**, 439–446 (2001).
6. B. R. Hammond, Jr., B. R. Wooten, and D. M. Snodderly, "Individual variations in the spatial profile of human macular pigment," *J. Opt. Soc. Am. A* **14**, 1187–1196 (1997).
7. D. M. Snodderly and B. R. Hammond, "*In vivo* psychophysical assessment of nutritional and environmental influences on human ocular tissues: lens and macular pigment," in *Nutritional and Environmental Influences on the Eye*, A. Taylor, Ed., pp. 251–273, CRC Press, Boca Raton, FL (1999).
8. J. S. Werner, M. L. Bieber, and B. E. Schefrin, "Senescence of foveal and parafoveal cone sensitivities and their relations to macular pigment density," *J. Opt. Soc. Am. A* **17**, 1918–1932 (2000).
9. P. E. Kilbride, K. R. Alexander, M. Fishman, and G. A. Fishman, "Human macular pigment assessed by imaging fundus reflectometry," *Vision Res.* **29**, 663–674 (1989).
10. R. W. Webb, G. W. Hughes, and F. C. Delori, "Confocal scanning laser ophthalmosope," *Appl. Opt.* **26**, 1492–1499 (1987).
11. F. C. Delori, D. G. Goger, B. R. Hammond, D. M. Snodderly, and S. A. Burns, "Macular pigment density measured by autofluorescence spectrometry: comparison with reflectometry and heterochromatic flicker photometry," *J. Opt. Soc. Am. A* **18**, 1212–1230 (2001).
12. W. Gellermann, I. V. Ermakov, M. R. Ermakova, R. W. McClane, D.-Y. Zhao, and P. S. Bernstein, "*In vivo* resonant Raman measurement of macular carotenoid pigments in the young and the aging human retina," *J. Opt. Soc. Am. A* **19**, 1172–1186 (2002).
13. I. V. Ermakov, R. W. McClane, W. Gellermann, N. Katz, and P. Bernstein, "Raman detection of human macula pigments," in *Proceedings of the International Conference on Lasers 98*, pp. 641–648, Society for Optical and Quantum Electronics, STS Press, McLean, VA (1999).
14. I. V. Ermakov, R. W. McClane, W. Gellermann, and P. S. Bernstein, "Resonant Raman detection of macular pigment levels in the living human retina," *Opt. Lett.* **26**, 202–204 (2001).
15. T. R. Hata, T. A. Scholz, I. V. Ermakov, R. W. McClane, F. Khachik, W. Gellermann, and L. K. Pershing, "Noninvasive Raman spectroscopic detection of carotenoids in human skin," *J. Invest. Dermatol.* **115**, 441–448 (2000).
16. I. V. Ermakov, M. R. Ermakova, R. W. McClane, and W. Gellermann, "Resonance Raman detection of carotenoid antioxidants in living human tissues," *Opt. Lett.* **26**, 1179–1181 (2001).
17. A. P. Shreve, J. K. Trautman, T. G. Owens, and A. C. Albrecht, "Determination of the S2 lifetime of β-carotene," *Chem. Phys. Lett.* **178**, 89 (1991).
18. Y. Koyama, I. Takatsuka, M. Nakata, and M. Tasumi, "Raman and infrared spectra of the all-*trans*, 7-*cis*, 9-*cis*, 13-*cis*, and 15-*cis* isomers of b-carotene: key bands distinguishing stretched or terminal-bent configurations from central-bent configurations," *J. Raman Spectrosc.* **19**, 37–49 (1988).
19. W. Gellermann, I. V. Ermakov, R. W. McClane, and P. S. Bernstein, "Raman detection of carotenoid pigments in the human retina," *Proc. SPIE* **3917**, 102–108 (2000).
20. American National Standards Institute, *Safe use of lasers*, Sec. 8.3, ANSI standard Z136.1-2000, Laser Institute of America, Orlando, FL (2000).
21. N. L. Mata, J. Weng, and G. H. Travis, "Biosynthesis of a major lipofuscin fluorophore in mice and humans with ABCR-mediated retinal and macular degeneration," *Proc. Natl. Acad. Sci. U.S.A.* **97**, 7154–7159 (2000).
22. G. Britton, S. Liaaen-Jensen, and H. Pfander, Eds., *Carotenoids*, Vol. 1B, *Spectroscopy*, Birkhauser Verlag, Basel, Switzerland (1995).
23. M. Born and E. Wolf, *Principles of Optics*, Pergamon Press, Oxford (1964).
24. G. Smith and D. A. Atchison, *The Eye and Visual Optical Instruments*, Cambridge University Press, Cambridge (1997).
25. P. S. Bernstein, D.-Y. Zhao, S. Wintch, I. Ermakov, R. McClane, and W. Gellermann, "Resonance Raman measurement of macular carotenoids in normal and age-related macular degeneration subjects," *Ophthalmology (Philadelphia)* **109**, 1780–1787 (2002).